

www.acsami.org Research Article

Facile Process for Fabrication of Silicon Micro-Nanostructures of Different Shapes as Molds for Fabricating Flexible Micro-Nanostructures and Wearable Sensors

Xiaoke Ding, Md Fazlay Rubby, Suya Que, Sajid Uchayash, and Long Que*



Cite This: https://doi.org/10.1021/acsami.2c22285

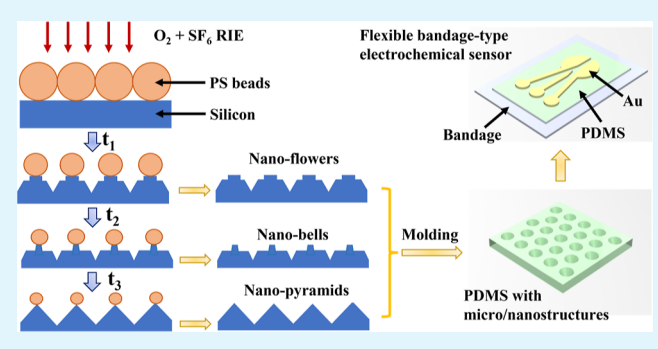


ACCESS I

III Metrics & More

Article Recommendations

ABSTRACT: We report a method to fabricate silicon micronanostructures of different shapes by tuning the number of layers and the sizes of self-assembled polystyrene beads, which serve as the mask, and by tuning the reactive ion etching (RIE) time. This process is simple, scalable, and inexpensive without using any sophisticated nanomanufacturing equipment. Specifically, in this work, we demonstrate the proposed process by fabricating silicon micro- or nanoflowers, micro- or nanobells, nanopyramids, and nanotriangles using a self-assembled monolayer or bilayer of polystyrene beads as the mask. We also fabricate flexible micronanostructures by using silicon molds with micronanostructures. Finally, we demonstrate the fabrication of bandage-type electro-



chemical sensors with micro—nanostructured working electrodes for detecting dopamine, a neurotransmitter related to stress and neurodegenerative diseases in artificial sweat. All these demonstrations indicate that the proposed process provides a low-cost, easy-to-use approach for fabricating silicon micro—nanostructures and flexible micro—nanostructures, thus paving a way for developing wearable micro—nanostructures enabled sensors for a variety of applications in an efficient manner.

KEYWORDS: self-assembled beads, silicon micro-nanostructures, flexible micro-nanostructures, wearable sensors, bandage sensors, neurotransmitter detection

1. INTRODUCTION

A variety of nanostructures have been fabricated using a topdown approach or synthesized using a bottom-up approach during the past decades. These nanoscale structures and devices not only have enabled advanced microelectronic devices in the semiconductor industry but also have formed the foundation for developing plasmonics, nanophotonics, and metamaterials, 11 just to name a few, for various applications. These applications span from bioscience, biomedical engineering, chemistry, medicine, and cancer therapy to energy harvesting and storage. 12-17 For instance, nanotubes can provide a unique platform for drug delivery, cell transfection, 18,19 and advanced patch-clamp recording techniques,²⁰ just to name a few. Specifically, by using the nanotubes as drug depots, more accurate and smaller amounts of drugs can be delivered and administered to the target locally. This could be very critical to control the drug dose and its release, thereby achieving optimal therapeutic effect while mitigating toxicity. Moreover, by taking advantage of the nanoscale size of the nanotubes to load biological cargos, negligible damage to the cell would be introduced when the nanotubes penetrate the cell membrane during a transfection procedure, and thus, the viability of cells would not be compromised. Using a nanotube

as a pipette in a patch-clamp technique, high-resolution monitoring of ion channels in cell membranes can be achieved, benefiting studies related to drug discovery targeted toward ion channelopathies and related diseases.^{20,21}

As aforementioned, different bottom-up approaches have been developed to synthesize different nanostructures from different materials, ¹⁻³ resulting in numerous exciting applications. Due to the high-temperature process and hence the incompatibility with integrated circuit microfabrication processes, often times it is very difficult to integrate the nanostructures such as carbon nanotubes synthesized in this way as functional components into a microdevice or microsystem in a controlled and simple manner. Hence, ideally the nanostructures can also be fabricated using a top-down approach. For the top-down approach, some mainly used

Received: December 10, 2022 Accepted: February 10, 2023



ACS Applied Materials & Interfaces

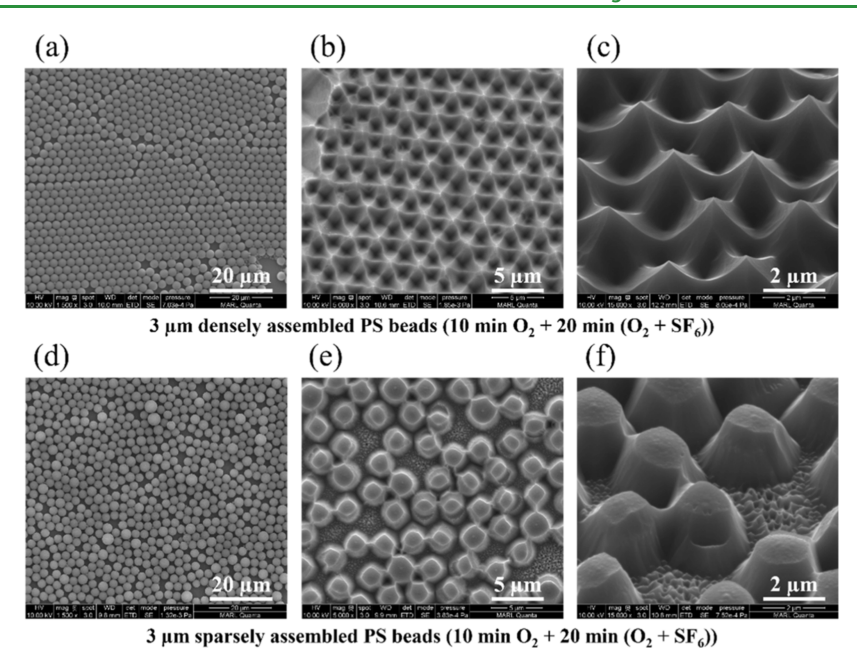


Figure 1. Effect of the densely and sparsely packed PS on the formation of silicon nanostructures. (a–c) SEM images of the densely assembled 3 μ m PS beads on the silicon surface and the fabricated silicon nanopyramids; (d–f) SEM images of sparsely assembled PS beads on the silicon surface and the fabricated silicon microcylinders.

techniques for fabricating nanostructures require sophisticated equipment and expensive nanolithography technologies, including electron beam lithography, extreme UV lithography, ion beam lithography, or scanning probe lithography. Meanwhile, in the past decades, other alternative approaches have been developed for fabricating nanodevices and nanostructures, such as nanoimprint lithography, low-cost self-assembly nanopatterning methods, and nanosphere lithography (NSL). NSL is enabled by colloidal solutions such as polystyrene or silica micro-/nanospheres, which can be self-assembled over large areas on a substrate in the form of a close-packed arrangement. The self-assembled spheres can be used as a shadow mask for deposition or as an etching mask. Using NSL, some nanostructures such as silicon pyramids were fabricated. Sp. We have fabricated silicon nanotubes by using the self-assembled nanosphere beads as the mask, followed by a deep reactive ion etching (RIE) process.

Herein, we report self-assembled polystyrene (PS) beadguided fabrication of silicon micro—nanostructures of different shapes by simply tuning the parameters of a RIE process and the number of layers of the self-assembled PS beads. We also report the fabrication of flexible polymer micro—nanostructures using micro—nanostructured silicon molds. In addition, development of a bandage-type electrochemical sensor enabled by the flexible micro—nanostructure for detecting a neurotransmitter dopamine has been demonstrated.

2. MATERIALS AND METHODS

2.1. Chemicals and Materials. The polystyrene nanosphere beads with different sizes (1000 and 3000 nm) were purchased from Fisher Scientific Inc. Triton X-100 and methanol were both purchased from Sigma-Aldrich Inc. Deionized (DI) water was obtained from a DI water purification system (Millipore, FRANCE). Silicon wafers were obtained from Ultrasil Corp. Chemicals for surface cleaning and treatment including acetone, IPA, 98% sulfuric acid, and 30% hydrogen peroxide were all obtained from Sigma-Aldrich Inc. Polydimethylsiloxane (PDMS) and its cure agents were purchased from Dow Corning (Midland, WI, USA). Dopamine hydrochloride

was purchased from Sigma-Aldrich, St. Louis, MO, USA. Artificial sweat was purchased from Reagents, Inc. Belmont, NC, USA.

2.2. Fabrication and Characterization of Silicon and Flexible Micro- or Nanostructures. First of all, one-side polished p-type 4 in. silicon wafers (Ultrasil Corp) are cut into 2 cm × 2 cm pieces. Then, each piece is cleaned by acetone, IPA, and DI water with the help of ultrasonication for 20 min in each solution in sequence. Then, the silicon pieces are immersed into a fresh piranha solution [a mixture of sulfuric acid and hydrogen peroxide (3:1)] in a beaker, which is kept on a hot plate at 60 °C for half an hour. Thereafter, the silicon pieces are taken out from the beaker and rinsed thoroughly by DI water. After the surface treatment, the silicon pieces can be used immediately or need to be stored in DI water to avoid formation of native oxide for future use. PS nanosphere beads are dispersed uniformly in a solution containing Triton X-100 and methanol (4% w/v PS beads in DI water/Triton X-100/methanol = 1000/1/10000, volume ratio). Then, a certain amount of PS bead solution is directly applied to each silicon piece by a micropipette. The solution is left to dry without any disturbance at room temperature for several hours. PS nanosphere beads are selfassembled into a close-packed monolayer. The beads are then tailored by oxygen plasma to shrink their size, and the gap among the PS nanospheres increases. Using the PS beads as the mask, O2 plasma etching is used to shrink the size of the PS beads, and RIE using a gas mixture of O2 and SF6 is used to etch silicon. After the RIE process, the silicon micro- or nanostructures are obtained by removing the residual PS beads from the surface of the silicon wafer using O2 plasma. Scanning electron microscopy (SEM) is used to image and evaluate the silicon micro- or nanostructures.

The flexible micro- or nanostructures are fabricated using soft lithograph process. 27 In the fabrication process, the silicon micro- or nanostructures are used as the mold. Briefly, liquid PDMS is first poured on the silicon mold, which is then followed by 1 h degassing and 2 h curing at 75 $^{\circ}\text{C}$. Afterward, the cured PDMS layer is peeled off from the mold, resulting in a layer of flexible micro–nanostructures. Again, SEM is used to image and evaluate the micro- or nanostructures transferred to the PDMS layer.

2.3. Fabrication of the Bandage-Type Sensors and Detection of Dopamine. Fabrication of bandage-type sensors involves two steps. First, the flexible micro- or nanostructures are fabricated on the PDMS layer using soft lithography, followed by fabricating a flexible three-electrode electrochemical sensor layer by

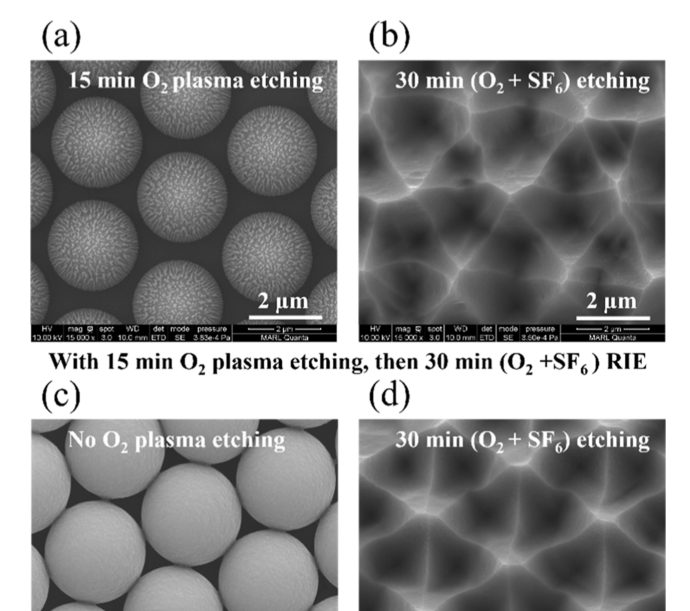
evaporating a layer of Au through a shadow mask. Then, the electrochemical sensor layer is bonded to a bandage (ScarAway, Inc.), forming a bandage-type electrochemical sensor. The detection of dopamine in the buffer and artificial sweat using the bandage sensor is performed by an Autolab PGSTAT204 potentiostat/galvanostat (Metrohm AG). Cyclic voltammetry (CV) and square wave voltammetry (SWV) analyses are performed through an Autolab PGSTAT204 potentiostat/galvanostat (Metrohm AG). The following parameters are used for CV: range, -0.4-+0.6 V; scan rate, 100 mV/s; incremental potential, 0.002 V. The following parameters are used for SWV: range, -0.5-+0.6 V; step, 0.005 V; modulation amplitude, 0.005 V; frequency, 8 Hz; duration, 27.25 s.

3. RESULTS AND DISCUSSION

3.1. Effects of PS Compactness and Size on Fabricating Silicon Nanostructures. First, the PS compactness, namely, the arrangement of the PS after being selfassembled on the silicon surface, on the silicon nanostructures as the mask has been evaluated. If the PS beads are densely assembled (i.e., closely packed) on the silicon surface as shown in Figure 1a as the mask, the silicon nanopyramids (Figure 1b,c) can be fabricated by oxygen plasma etching for 10 min to tailor the size of the PS beads, followed by RIE using a mixture of O2 and SF6 gas species for 20 min. In contrast, if the PS bead suspension has a lower concentration or a smaller amount, the PS beads are sparsely assembled (i.e., sparsely packed) on the silicon surface, as shown in Figure 1d, as the mask, and the silicon nanopyramids cannot be fabricated using the same processes. Instead, randomly distributed or disorderly distributed silicon micro- or nanocylinders (Figure 1e,f) have been fabricated. Hence, in the experiments, to fabricate uniformly arranged silicon micro-nanostructures, the densely assembled PS beads on the silicon wafers will be used as the

Second, two different manufacturing process flows for fabricating silicon nanopyramids have been evaluated: (i) PROCESS-I: The sizes of PS beads are tailored by oxygen plasma etching, followed by RIE of a gas mixture of O₂ and SF₆ to fabricate the silicon nanopyramids. (ii) PROCESS-II: RIE of a gas mixture of O2 and SF6 to fabricate the silicon nanopyramids. As shown in Figure 2a, the sizes of PS beads are reduced after 15 min O₂ plasma etching, resulting in gaps among the PS beads. The silicon nanopyramids are fabricated by 30 min RIE by a gas mixture of O₂ and SF₆, which is shown in Figure 2b after the PS beads are removed. The silicon nanopyramids can also be fabricated without tailoring the sizes of the PS beads. As shown in Figure 2c,d, RIE of a gas mixture of O₂ and SF₆ is directly carried out on a PS beads-masked silicon wafer, and the silicon nanopyramids can also be fabricated. This process (PROCESS-II) flow can simplify the fabrication procedure. Even though without the step to shrink the sizes of the PS beads, the silicon underneath the PS beads can be effectively removed by RIE enabled by a mixture of O₂ and SF₆ gas species.

3.2. Fabricated Silicon Micro-Nanostructures of Different Shapes. 3.2.1. Silicon Micro-anostructures Fabricated by Different RIE Times Using a Single Monolayer of PS Beads as the Mask. Using the PROCESS-II, by tuning the RIE etching time (Figure 3a), micro-nanostructures of different shapes can be fabricated consistently. Increased RIE time results in increased removal of the silicon underneath the PS beads. Given the isotropic nature of the RIE, namely, the lateral etching of the silicon besides the vertical etching of the silicon relative to the surface of a silicon wafer by RIE, silicon



Without O₂ plasma etching, 30 min (O₂ +SF₆) RIE

Figure 2. Effect of shrinking size of PS on the formation of silicon nanostructures. SEM images of (a) 3 μ m PS beads assembled on the silicon surface after 15 min O₂ plasma etching and (b) fabricated silicon nanopyramids. SEM images of (c) 3 μ m PS beads assembled on the silicon surface and (d) fabricated silicon nanopyramids.

micro–nanoflowers, silicon micro–nanobells, and silicon nanopyramids will be formed with increased etching time in sequence. Some representative SEM images of the fabricated micro–nanostructures are shown in Figure 3b. In this case, the sizes of the PS beads are 3 μ m. The silicon microflowers are formed after 5 min RIE, microbells are formed after 10 min RIE, and nanopyramids are formed after 20 min RIE.

PROCESS-I has also been used to evaluate the fabrication of microbells using 3 μ m PS beads as the mask. As shown in Figure 3c, after 5, 10, and 15 min O₂ plasma etching to shrink the sizes of the PS beads, the microbells can be fabricated by 10 min RIE of a gas mixture (O₂ and SF₆), again indicating that both PROCESS-I and PROCESS-II can fabricate the targeted silicon microstructures. To further scale down the sizes of these silicon structures, 1 μ m PS beads are used as the mask, as shown in Figure 3d, and the nanoflowers, nanobells, and nanopyramids can be successfully fabricated. Note that the RIE time has been reduced to 1, 2, and 4 min to fabricate nanoflowers, nanobells, and nanopyramids, respectively, compared to those with 3 μ m PS beads as the mask.

3.2.2. Nanostructures Fabricated by Two Layers of PS Beads as the Mask. Two layers of 1 μ m PS beads are self-assembled on the silicon surface by applying PS beads twice on the silicon wafer as shown in Figure 4a—c. To verify there are two layers of PS beads, oxygen plasma etching is performed to shrink the size of the beads so that the layer of beads underneath can be observed. As shown in Figure 4c, with the removal of the beads from the top layer, the PS beads underneath can be clearly observed. PROCESS-I and PROCESS-II are used to fabricate the nanostructures with two layers of 1 μ m PS beads as the mask, respectively. A representative SEM image of PS beads after PROCESS-I is

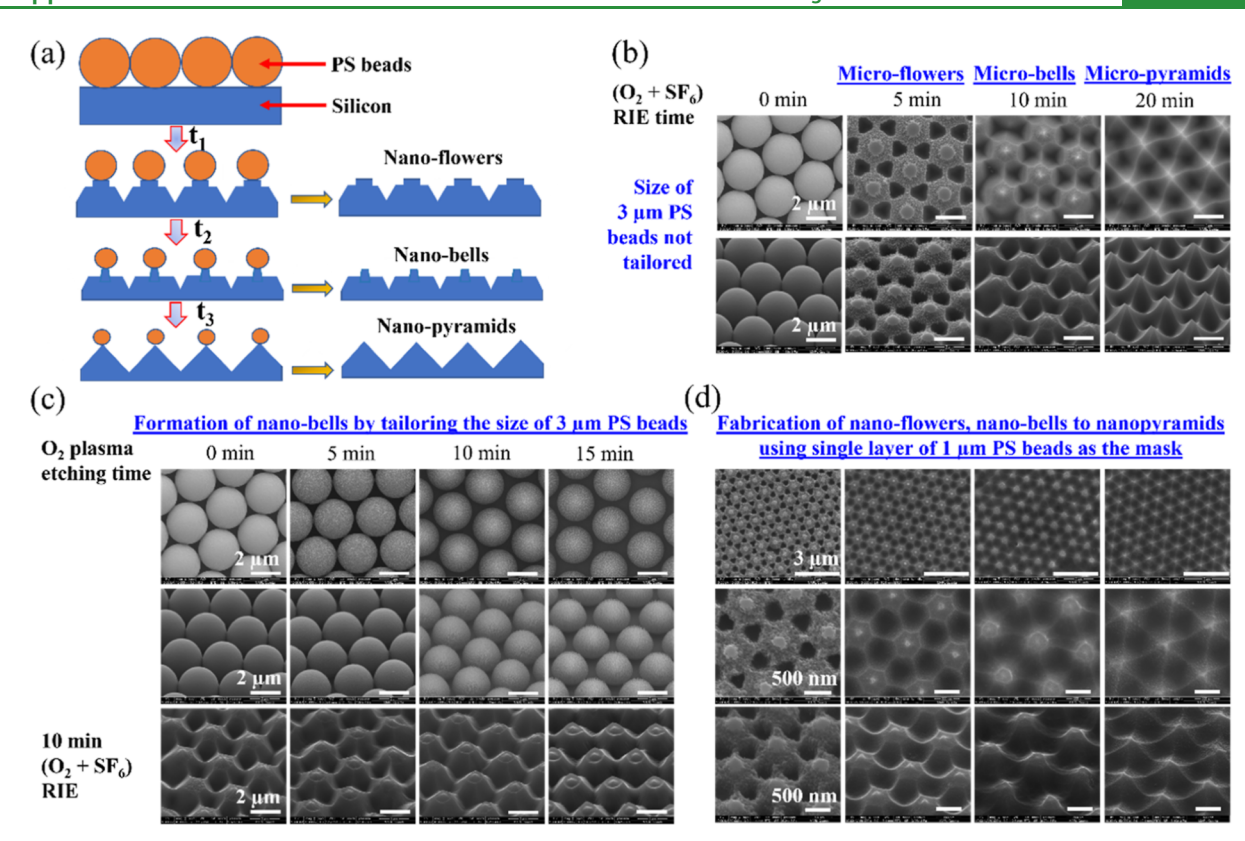


Figure 3. Fabricating micro- and nanostructures of different shapes by tuning the RIE time. (a) Schematic illustration of fabricating micro- or nanoflowers, micro- or nanobells, and nanopyramids with different RIE ($O_2 + SF_6$) times; (b) top row (top view) and bottom row (angled view): SEM images of PS beads, microflowers, microbells, and micropyramids fabricated using PROCESS-II with 3 μ m PS beads as the mask; (c) top row (top view) and middle row (angled view): SEM images of PS beads after O_2 plasma etching with different times; bottom-row (angled view): the corresponding SEM images of microbells fabricated using 10 min RIE ($O_2 + SF_6$); (d) top row (top view), middle row (top view, close up), and bottom row (angled view): SEM images of nanoflowers, nanobells, and nanopyramids fabricated using PROCESS-II with 1 μ m PS beads as the mask.

shown in Figure 4d. The silicon nanotriangles are fabricated underneath the PS beads. After the PS beads are removed, silicon nanotriangles have been fabricated as shown in Figure 4g,h. Some representative SEM images of silicon nanotriangles fabricated using PROCESS-II are shown in Figure 4e,f. As can be seen clearly, there are silicon nanoislands among three nanotriangles in Figure 4e,f. In contrast, no nanoislands exist in Figure 4g,h. The formation of the silicon nanotriangles and nanoislands can be explained using the schematic illustration in Figure 4i-k. As shown in Figure 4i, arrayed triangle openings are formed among the highly packed PS beads, and the size of triangle openings reduced with the second layer of the highly packed PS beads as shown in Figure 4j. With these PS beads as the mask, using PROCESS-II, the nanotriangles can be fabricated through the triangle-shape openings through the PS beads. Meanwhile, the size of each PS bead is still big enough to mask the underneath silicon to avoid the silicon to be totally etched away, resulting in the nanoisland (Figure 4e,f). In contrast, using PROCESS-I, the size of the top-layer PS beads has been shrunk (Figure 4k), while the nanotriangles can be fabricated, and the size of the top-layer PS beads is not big enough to mask the underneath silicon. As a result, the underneath silicon will be etched away, and no nanoislands exist (Figure 4g,h).

3.3. Fabricated Flexible Micro- and Nanostructures. The fabricated silicon micro- or nanostructures can be used as a mold to fabricate the flexible and inversed micro- or nanostructures. The process flow is illustrated in Figure 5a-c.

A liquid polydimethylsiloxane mixture (Sylgard 184) was prepared by mixing the base and cure agent with a ratio of 10:1. Then, the liquid mixture was poured onto a silicon mold, followed by baking at 75 °C for 2 h. The cured PDMS layer was peeled off the master mold, and the micro- or nanostructures were transferred to the PDMS layer. A photo of a PDMS layer with transferred micro- or nanostructures is shown in Figure 5d. Three types of silicon molds have been used to fabricate flexible micro- and nanostructures. As shown in Figure 5e, using the silicon molds with microflowers, microbells, and nanopyramids, the inversed microstructures can be transferred to the PDMS layer with high fidelity. For the silicon molds with nanoflowers, nanobells, and nanopyramids in Figure 5f, the fidelity of the transferred inversed nanostructures degraded somewhat, but the main features remain reasonably good. The nanotriangles from the silicon mold have been also successfully transferred to the PDMS layer with nanotriangle islands as shown in Figure 5g.

3.4. Detection of Dopamine Using Bandage-Type Sensors. It has been found that the dopamine levels and dopaminergic neuronal activity in the mesolimbic dopamine system are affected by stress, ²⁸ in addition to other diseases such as Parkinson's disease. ²⁹ These changes in mesolimbic dopaminergic neurotransmission, allowing adaption to behavioral responses to environmental stimuli, are important for coping with stress. Monitoring dopamine levels in sweat is attractive since the measurement can be taken noninvasively and in real time. ³⁰ As a technical demonstration, herein, the

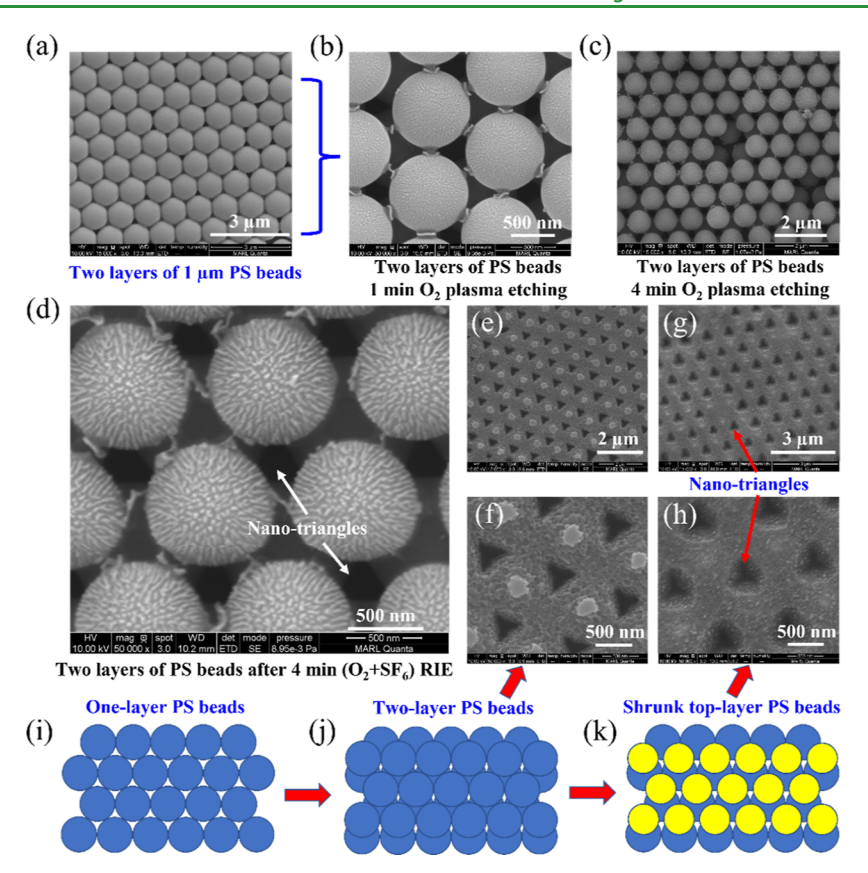


Figure 4. Fabrication of silicon nanotriangles using two layers of 1 μ m PS beads as the mask. SEM images of (a) two-layer 1 μ m PS beads, (b) PS beads after 1 min O₂ plasma etching, and (c) PS beads after 4 min O₂ plasma etching. The PS beads underneath are clearly observed; (d) nanotriangles fabricated underneath PS beads; (e,f) nanotriangles fabricated using PROCESS II; (g,h) nanotriangles fabricated using PROCESS I. (i,k) Schematic illustration of fabricating nanotriangles using two-layer 3 μ m PS beads.

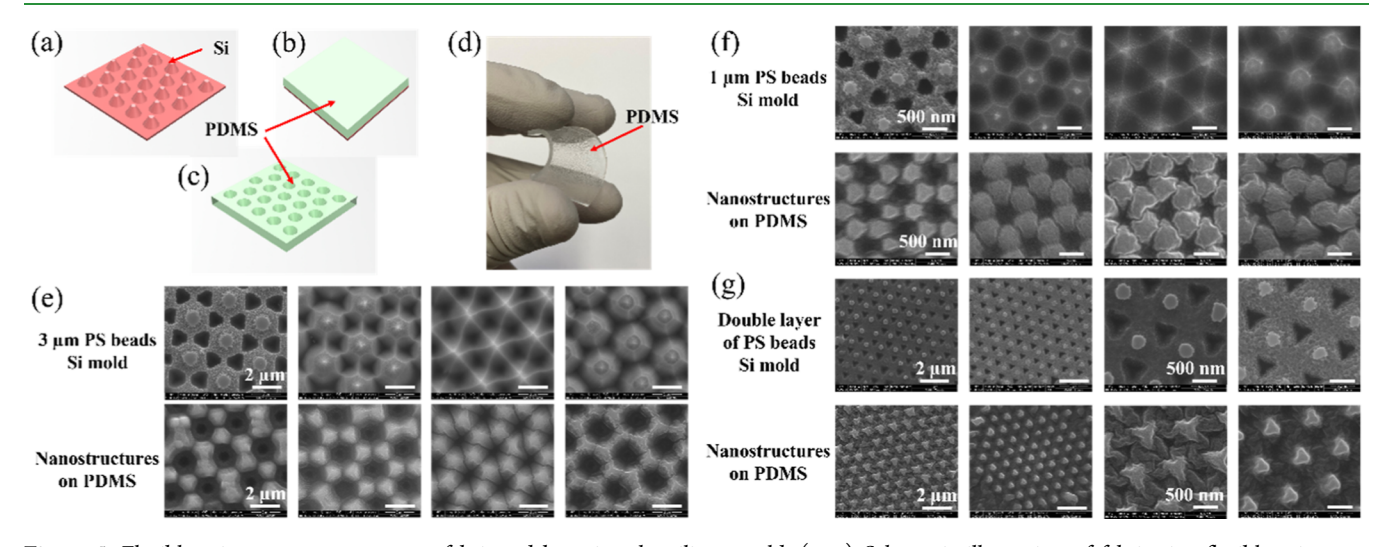


Figure 5. Flexible micro- or nanostructures fabricated by using the silicon mold. (a–c) Schematic illustration of fabricating flexible micro- or nanostructures using the silicon mold; (d) photo of a flexible micro- or nanostructure fabricated on PDMS; (e) top row: SEM images of micro-nanostructures on the silicon mold; bottom row: SEM images of inversed micro-nanostructures corresponding to those on the silicon mold; (f) top row: SEM images of nanostructures on the silicon mold; bottom row: SEM images of inversed nanostructures corresponding to those on the silicon mold; (g) top row: SEM images of nanostructures on the silicon mold; bottom row: SEM images of inversed nanostructures corresponding to those on the silicon mold.

bandage sensors fabricated using the silicon mold to detect dopamine are demonstrated.

The process flow chart for fabricating bandage sensors is illustrated in Figure 6a-d. Briefly, the micro-nanostructures are transferred to a PDMS layer. Then, a shadow mask is put

on top of the PDMS layer. Then, 100 nm thick Au is deposited on the PDMS layer through the shadow mask. Afterward, the shadow mask is removed, followed by bonding the Au-coated three-electrode electrochemical sensor to the bandage (Scar-Away, Inc.) as shown in Figure 6e. The measured currents of

www.acsami.org

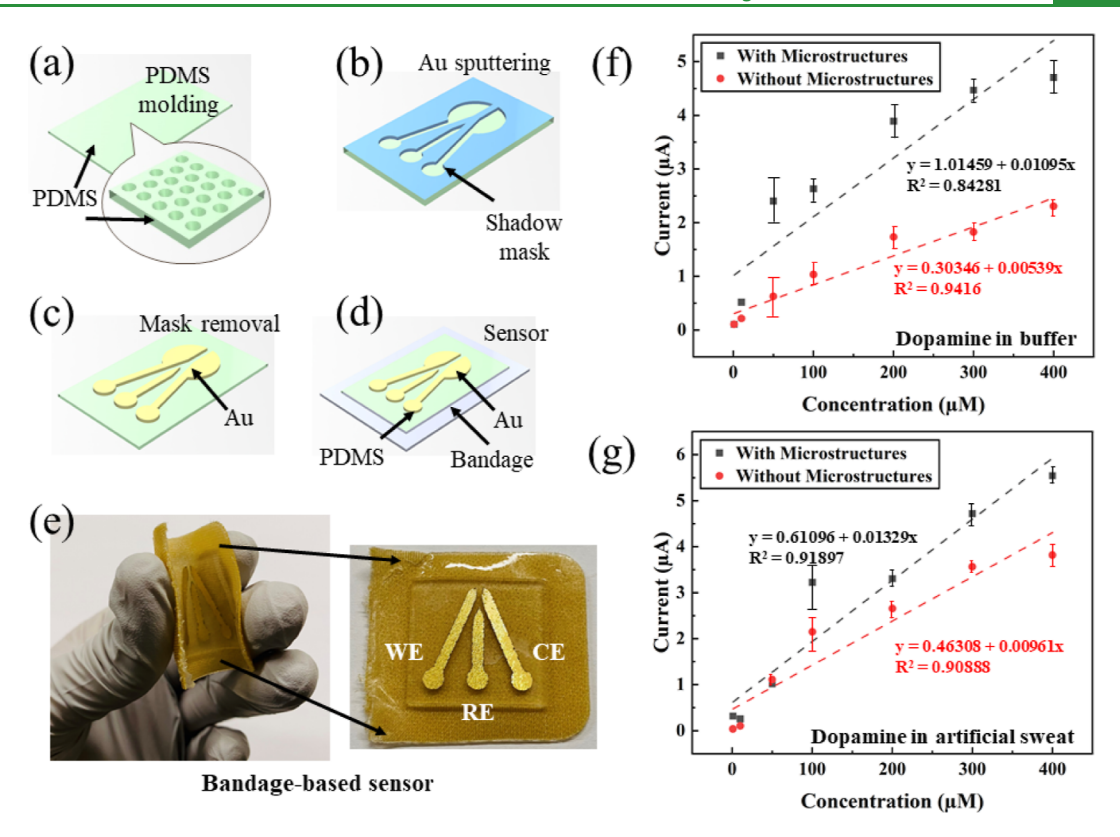


Figure 6. Fabrication of the bandage sensor and detection of dopamine in artificial sweat. (a–d) Schematic illustration of fabricating bandage sensors; (e) photo of a fabricated bandage electrochemical sensor; (f) transducing signals of different levels of dopamine in buffer for bandage sensors using the micro–nanostructured WE in comparison to the planar WE; (g) transducing signals of different levels of dopamine in artificial sweat for bandage sensors using the micro–nanostructured WE in comparison to the planar WE. Error bars were obtained by calculating standard deviation values.

dopamine in buffer (PBS) of different concentrations are shown in Figure 6f. The sensors with a micro—nanostructured working electrode (WE) offer enhanced signals (~2 fold) compared to the sensors with a planar WE. The measured currents of dopamine in the artificial sweat of different concentrations are shown in Figure 6g. The sensors with the micro—nanostructured WE also offer enhanced signals compared to the sensors with the planar WE. The enhanced transducing signals (i.e., peak currents) are due to the enhanced surface areas for the micro—nanostructured WE compared to those of the planar WE, which is consistent to those reported in previous work.³¹

4. CONCLUSIONS

In this paper, silicon micro- or nanostructures of different shapes have been fabricated using self-assembled PS beads on silicon wafer as the mask. Specifically, by tuning the silicon etching time, microscale or nanoscale flowers, bells, and nanopyramids can be fabricated with one layer of PS beads as the mask. The silicon nanotriangles have been fabricated using two-layer self-assembled PS beads on silicon wafer as the mask. Using these silicon molds with micro- or nanostructures, the flexible micro- or nanostructures have been fabricated. Furthermore, bandage-type electrochemical sensors have been fabricated using the silicon molds with micro- or nanostructures for detecting dopamine in buffer and artificial sweat, which show enhanced transducing signals of the electrochemical sensors with micro- or nanostructure-based WE. Given its simple-to-use and low-cost, this manufacturing process provides a new method to fabricate silicon and flexible

micro- or nanostructures of different shapes in an efficient manner, paving a way to develop wearable micro- or nanosensors with enhanced performance for biomedical and healthcare applications.

AUTHOR INFORMATION

Corresponding Author

Long Que — Department of Electrical and Computer Engineering, Iowa State University, Ames, Iowa 50011, United States; orcid.org/0000-0002-1603-4219; Email: lque@iastate.edu

Authors

Xiaoke Ding — Department of Electrical and Computer Engineering, Iowa State University, Ames, Iowa 50011, United States

Md Fazlay Rubby — Department of Electrical and Computer Engineering, Iowa State University, Ames, Iowa 50011, United States

Suya Que – School of Engineering and Applied Science, University of Pennsylvania, Philadelphia, Pennsylvania 19104, United States

Sajid Uchayash — Department of Electrical and Computer Engineering, Iowa State University, Ames, Iowa 50011, United States

Complete contact information is available at: https://pubs.acs.org/10.1021/acsami.2c22285

Notes

The authors declare no competing financial interest.

ACKNOWLEDGMENTS

We would like to thank the technical staffs at Microelectronics Research Center (MRC) and Dr. Warren Straszheim at MARL, Iowa State University for their technical support. This research was funded in part by the Exploratory Research Program at the Iowa State University and NSF CMMI 2031826.

REFERENCES

- (1) Maschmann, M. R.; Amama, P. B.; Goyal, A.; Iqbal, Z.; Fisher, T. S. Freestanding Vertically Oriented Single-Walled Carbon Nanotubes Synthesized Using Microwave Plasma-Enhanced CVD. *Carbon* **2006**, 44, 2758–2763.
- (2) Goldberger, J.; He, R.; Zhang, Y.; Lee, S.; Yan, H.; Choi, H.-J.; Yang, P. Single-Crystal Gallium Nitride Nanotubes. *Nature* **2003**, 422, 599–602.
- (3) Goldberger, J.; Fan, R.; Yang, P. Inorganic Nanotubes: A Novel Platform for Nanofluidics. *Acc. Chem. Res.* **2006**, *39*, 239–248.
- (4) Sha, J.; Niu, J.; Ma, X.; Xu, J.; Zhang, X.; Yang, Q.; Yang, D. Silicon Nanotubes. *Adv. Mater.* **2002**, *14*, 1219–1221.
- (5) Perepichka, D. F.; Rosei, F. Silicon Nanotubes. *small* 2006, 2, 22-25.
- (6) Favors, Z.; Wang, W.; Bay, H. H.; George, A.; Ozkan, M.; Ozkan, C. S. Stable Cycling of SiO2 Nanotubes as High-Performance Anodes for Lithium-Ion Batteries. *Scientific reports* **2014**, *4*, 1–7.
- (7) He, Y.; Che, X.; Que, L. A Top-Down Fabrication Process for Vertical Hollow Silicon Nanopillars. *Journal of Microelectromechanical systems* **2016**, *25*, 662–667.
- (8) Peer, E.; Artzy-Schnirman, A.; Gepstein, L.; Sivan, U. Hollow Nanoneedle Array and Its Utilization for Repeated Administration of Biomolecules to the Same Cells. *ACS Nano* **2012**, *6*, 4940–4946.
- (9) Rycenga, M.; Cobley, C. M.; Zeng, J.; Li, W.; Moran, C. H.; Zhang, Q.; Qin, D.; Xia, Y. Controlling the Synthesis and Assembly of Silver Nanostructures for Plasmonic Applications. *Chemical reviews* **2011**, *111*, 3669–3712.
- (10) Lindquist, N. C.; Nagpal, P.; McPeak, K. M.; Norris, D. J.; Oh, S.-H. Engineering Metallic Nanostructures for Plasmonics and Nanophotonics. *Reports on Progress in Physics* **2012**, *75*, 036501.
- (11) Yang, K.-C.; Puneet, P.; Chiu, P.-T.; Ho, R.-M. Well-Ordered Nanonetwork Metamaterials from Block Copolymer Templated Syntheses. *Acc. Chem. Res.* **2022**, *55*, 2033–2042.
- (12) Ghadamgahia, M.; Ajloo, D.; Alipour, Y. How Do Palladium Complexes Affect on Coil Structure of Human Serum Albumin in the Presence of Carbon Nanotube? A Molecular Dynamics Study. *Physical Chemistry Research* **2016**, *4*, 47–60.
- (13) Roosta, S.; Hashemianzadeh, S. M.; Ketabi, S. Encapsulation of Cisplatin as an Anti-Cancer Drug into Boron-Nitride and Carbon Nanotubes: Molecular Simulation and Free Energy Calculation. *Materials Science & Engineering C-Materials for Biological Applications* **2016**. *67*, 98–103.
- (14) Singh, R. P.; Sharma, G.; Sonali; Singh, S.; Patne, S. C. U.; Pandey, B. L.; Koch, B.; Muthu, M. S. Effects of Transferrin Conjugated Multi-Walled Carbon Nanotubes in Lung Cancer Delivery. Materials Science & Engineering C-Materials for Biological Applications 2016, 67, 313–325.
- (15) Xie, C. L.; Li, P.; Liu, Y.; Luo, F.; Xiao, X. F. Preparation of TiO2 Nanotubes/Mesoporous Calcium Silicate Composites with Controllable Drug Release. *Materials Science & Engineering C-Materials for Biological Applications* **2016**, 67, 433–439.
- (16) Zhang, H.; Cao, G.; Wang, Z.; Yang, Y.; Shi, Z.; Gu, Z. Growth of Manganese Oxide Nanoflowers on Vertically-Aligned Carbon Nanotube Arrays for High-Rate Electrochemical Capacitive Energy Storage. *Nano Lett.* **2008**, *8*, 2664–2668.
- (17) Hu, R.; Cola, B. A.; Haram, N.; Barisci, J. N.; Lee, S.; Stoughton, S.; Wallace, G.; Too, C.; Thomas, M.; Gestos, A.; Cruz, M. E. d.; Ferraris, J. P.; Zakhidov, A. A.; Baughman, R. H. Harvesting Waste Thermal Energy Using a Carbon-Nanotube-Based Thermo-Electrochemical Cell. *Nano Lett.* **2010**, *10*, 838–846.

- (18) Golshadi, M.; Wright, L. K.; Dickerson, I. M.; Schrlau, M. G. High-Efficiency Gene Transfection of Cells through Carbon Nanotube Arrays. *Small* **2016**, *12*, 3014–3020.
- (19) Nia, A. H.; Amini, A.; Taghavi, S.; Eshghi, H.; Abnous, K.; Ramezani, M. A facile Friedel-Crafts Acylation for the Synthesis of Polyethylenimine-Grafted Multi-Walled Carbon Nanotubes as Efficient Gene Delivery Vectors. *Int. J. Pharm.* **2016**, *502*, 125–37.
- (20) Duan, X.; Lieber, C. M. Nanoscience and the Nano-Bioelectronics Frontier. *Nano Res.* **2015**, *8*, 1–22.
- (21) Catterall, W. A.; Dib-Hajj, S.; Meisler, M. H.; Pietrobon, D. Inherited Neuronal Ion Channelopathies: New Windows on Complex Neurological Diseases. *J. Neurosci.* **2008**, 28, 11768–11777.
- (22) Chou, S. Y.; Krauss, P. R.; Renstrom, P. J. Nanoimprint Lithography. Journal of Vacuum Science & Technology B: Microelectronics and Nanometer Structures Processing, Measurement, and Phenomena 1996, 14, 4129–4133.
- (23) van Dommelen, R.; Fanzio, P.; Sasso, L. Surface Self-Assembly of Colloidal Crystals for Micro-and Nano-Patterning. *Advances in colloid and interface science* **2018**, 251, 97–114.
- (24) Hulteen, J. C.; Van Duyne, R. P. Nanosphere lithography: A Materials General Fabrication Process for Periodic Particle Array Surfaces. *Journal of Vacuum Science & Technology A: Vacuum, Surfaces, and Films* **1995**, *13*, 1553–1558.
- (25) Zhou, S.; Yang, Z.; Gao, P.; Li, X.; Yang, X.; Wang, D.; He, J.; Ying, Z.; Ye, J. Wafer-Scale Integration of Inverted Nanopyramid Arrays for Advanced Light Trapping in Crystalline Silicon Thin Film Solar Cells. *Nanoscale research letters* **2016**, *11*, 1–8.
- (26) Garín, M.; Khoury, R.; Martín, I.; Johnson, E. Direct Etching at the Nanoscale Through Nanoparticle-Directed Capillary Condensation. *Nanoscale* **2020**, *12*, 9240–9245.
- (27) Ding, X.; Ben-Shlomo, G.; Que, L. Soft Contact Lens With Embedded Microtubes for Sustained and Self-Adaptive Drug Delivery for Glaucoma Treatment. ACS Appl. Mater. Interfaces 2020, 12, 45789–45795.
- (28) Baik, J.-H. Stress and the Dopaminergic Reward System. Experimental & Molecular Medicine 2020, 52, 1879—1890.
- (29) Piggott, M.; Marshall, E.; Thomas, N.; Lloyd, S.; Court, J.; Jaros, E.; Burn, D.; Johnson, M.; Perry, R.; McKeith, I.; Ballard, C.; Perry, E. K. Striatal Dopaminergic Markers in Dementia With Lewy Bodies, Alzheimer's and Parkinson's Diseases: Rostrocaudal Distribution. *Brain* 1999, 122, 1449–1468.
- (30) Lei, Y.; Butler, D.; Lucking, M. C.; Zhang, F.; Xia, T.; Fujisawa, K.; Granzier-Nakajima, T.; Cruz-Silva, R.; Endo, M.; Terrones, H.; Terrones, M.; Ebrahimi, A. Single-Atom Doping of MoS2 With Manganese Enables Ultrasensitive Detection of Dopamine: Experimental and Computational Approach. *Science advances* **2020**, *6*, No. eabc4250.
- (31) Senel, M.; Dervisevic, M.; Alhassen, S.; Alachkar, A.; Voelcker, N. H. Electrochemical Micropyramid Array-Based Sensor for In Situ Monitoring of Dopamine Released from Neuroblastoma Cells. *Anal. Chem.* **2020**, 92, 7746–7753.